PHYSICAL REVIEW B **89**, 245112 (2014)

Spin-liquid phase in a spatially anisotropic frustrated antiferromagnet: A Schwinger boson mean-field approach

Jaime Merino
Departamento de Física Teórica de la Materia Condensada, Condensed Matter Physics Center (IFIMAC) and Instituto Nicolás Cabrera, Universidad Autónoma de Madrid, Madrid 28049, Spain

Michael Holt and Ben J. Powell
School of Mathematics and Physics, University of Queensland, Brisbane, 4072 Queensland, Australia
(Received 18 February 2014; revised manuscript received 25 April 2014; published 10 June 2014)

We explore the effect of the third-nearest neighbors on the magnetic properties of the Heisenberg model on an anisotropic triangular lattice. We obtain the phase diagram of the model using Schwinger boson mean-field theory. Competition between Néel, spiral, and collinear magnetically ordered phases is found as we vary the ratios of the nearest J_1, next-nearest J_2, and third-nearest J_3 neighbor exchange couplings. A spin-liquid phase is stabilized between the spiral and collinear ordered states when $J_2/J_1 \gtrsim 1.8$, for rather small $J_3/J_1 \lesssim 0.1$. The lowest-energy two-spinon dispersions relevant to neutron scattering experiments are analyzed and compared to semiclassical magnon dispersions finding significant differences in the spiral and collinear phases between the two approaches. The results are discussed in the context of the anisotropic triangular materials: Cs_2CuCl_4 and Cs_2CuBr_4 and layered organic materials, κ-(BEDT-TTF)$_2X$, and Y[Pd(dmit)$_2$]$_2$.

DOI: 10.1103/PhysRevB.89.245112 PACS number(s): 75.10.Jm, 75.10.Kt, 71.27.+a

I. INTRODUCTION

Quantum spin liquids (QSL) are exotic states of matter with no broken symmetries even at zero temperature [1]. Fractional excitations such as deconfined spin $S = \frac{1}{2}$ spinons are expected to occur as well as emergent gauge fields. These exotic phenomena are typically explored in low-dimensional $S = \frac{1}{2}$ systems. However, understanding the precise conditions for the realization of a QSL is a major challenge in theoretical condensed matter physics. For instance, in the one-dimensional $S = 1/2$ Heisenberg model, low-energy magnetic excitations are not the conventional $S = 1$ magnons expected in an ordered magnet [2] but $S = 1/2$ spinons which propagate as domain walls along the chain [3]. While this is a well-understood example of fractionalization, the existence of such fractional excitations in a two-dimensional spin system remains unsettled.

As well as the fundamental theoretical interest further impetus to investigate QSLs has arisen from recent experimental observations identifying several materials in which such unconventional behavior may be realized. The κ-(BEDT-TTF)$_2X$ and Y[Pd(dmit)$_2$]$_2$ families of organic charge-transfer salts include spin-liquid materials such as κ-(BEDT-TTF)$_2$Cu$_2$(CN)$_3$ and Me$_3$EtSb[Pd(dmit)$_2$]$_2$ where Et = C_2H_5 and Me = CH_3 in contrast to other antiferromagnetically ordered Mott insulators such as the X = Cu[N(CN)$_2$]Cl salts. There have also been predictions of a spin liquid in Mo_3S_7(dmit)$_3$, where the molecules themselves provide a triangular motif [4]. There are also a number of possible spin liquids in inorganic materials. Cs_2CuCl_4 does not display spiral magnetic order down to $T = 0.62$ K and Cs_2CuBr_4 is also a candidate system for spin-liquid behavior. Both the organic and inorganic materials discussed above have been primarily modeled in terms of the Heisenberg model on an anisotropic triangular lattice with exchange constants J_1 and J_2. The organic materials κ-(BEDT-TTF)$_2$Cu$_2$(CN)$_3$ and Me$_3$EtSb[Pd(dmit)$_2$]$_2$ are in the regime [5] $J_2/J_1 \approx 0.7$, whereas Cs_2CuCl_4 ($J_2/J_1 \approx 3$) and Cs_2CuBr_4 ($J_2/J_1 \approx 2$) are closer to the weakly coupled chain limit [6]. Other materials which may display spin-liquid behavior are $Ba_3CoSb_2O_9$ (Ref. [7]) and $Ba_3CuSb_2O_9$ (Ref. [8]) which have isotropic triangular lattices [9] $J_2/J_1 = 1$.

There are several experimental observations which suggest the existence of spin-liquid behavior in these materials. Susceptibility and NMR measurements in κ-(BEDT-TTF)$_2$Cu$_2$(CN)$_3$ and $Ba_3CuSb_2O_9$ find no magnetic order down to very low temperatures [10], much lower than J_1. The specific heat probing magnetic excitations reveals a linear temperature dependence [10] in such Mott insulators, suggesting the existence of a Fermi surface consisting of fractional excitations (spinons) [11,12]. In κ-(BEDT-TTF)$_2$Cu$_2$(CN)$_3$, a power-law T dependence $1/T_1 \propto T^{3/2}$ below 1 K [13] is observed. The absence of magnetic order together with the power-law T dependence suggest the vanishing of the gap to triplet excitations [10,14]. NMR experiments on Cs_2CuCl_4 show [15,16] a linear dependence of the relaxation rate with temperature $1/T_1 \propto T$ in the short-range ordered region $T > 0.62$ K. In the same temperature regime, neutron scattering experiments observe a continuum of excitations consistent with the presence of deconfined spinons [17].

The above unconventional behavior is difficult to understand theoretically. For instance, there is overwhelming numerical evidence that the Heisenberg model on an isotropic triangular lattice has the 120° Néel ordered state [18,19] as the ground state in contrast to Anderson's original prediction for a spin liquid [20]. This seems consistent with the antiferromagnetic (AF) order observed in the nearly isotropic organic materials [5]: Me$_4$Sb[Pd(dmit)$_2$]$_2$ and Me$_2$Et$_2$As[Pd(dmit)$_2$]$_2$. However, it is inconsistent with observations in isotropic triangular lattice materials: $Ba_3CoSb_2O_9$ [7] and $Ba_3CuSb_2O_9$. Hence, other interaction terms not present in the nearest-neighbor Heisenberg model should be included to explain discrepancies with the observations [5].

One possible route to spin-liquid behavior is the presence of further neighbor AF exchange couplings not considered in

the nearest-neighbor models. These can be generated through the, second-order, exchange mechanism, i.e., $J_3 \propto t_3^2/U$, where t_3 is the hopping integral between third-neighboring sites. Alternatively, fourth-order processes can give rise to a $J_3 \propto t_1^2 t_2^2/U^3$, where t_1 and t_2 are the nearest- and next-nearest-neighbor hopping integrals. These fourth-order processes also give rise to a ring exchange term $J_3(\mathbf{S}_i \cdot \mathbf{S}_j)(\mathbf{S}_k \cdot \mathbf{S}_l)$, where $\mathbf{S}_i$ is the Heisenberg spin operator on the ith site.

Second- and third-nearest-neighbor AF exchange coupling frustrates magnetically ordered phases and can lead to spin-liquid behavior. For instance, Wang and Vishwanath [21] have found spin-disordered flux phases in the large quantum fluctuation regime effectively corresponding to spins smaller than $\frac{1}{2}$. Ring exchange can also lead to spin-liquid behavior on the isotropic triangular [12,22] and anisotropic triangular lattices [23]. On the isotropic triangular lattice, the two contributions generated by fourth-order processes lead to spin-liquid behavior (for $J_3/J_1 > 0.1$) which is characterized by gapless magnetic excitations and a spinon Fermi surface [12]. It is then interesting to understand the effect of each contribution separately. Alternatively, other mechanisms may also stabilize spin liquids. For example, it has been argued that the Dzyaloshinskii-Moriya interaction may also produce a spin-liquid behavior in kagome lattices [24] and anisotropic triangular lattices [6].

The main aim of this work is to analyze the effect of next-nearest-neighbor interaction J_3 on the magnetic properties of the Heisenberg model on anisotropic triangular lattices. Since these interactions can be generated by fourth-order processes that also lead to ring exchange as discussed above, our work contributes to the general understanding of ring-exchange effects on frustrated antiferromagnets [23]. We use Schwinger boson mean-field theory (SB-MF) [25] expressed in terms of antiferromagnetic and ferromagnetic bonds which are treated as variational parameters [26–28]. The Schwinger boson approach is particularly useful since it can describe ordered and disordered phases on equal footing; the magnetically ordered phases resulting from the condensation of the bosons at particular order wave vectors of the system. We find that when the anisotropy $J_2/J_1 \gtrsim 1.8$ of the system is amenable to spin-liquid behavior under the effect of a weak next-nearest-neighbor interaction, $J_3/J_1 \lesssim 0.1$. Since these results are obtained from Schwinger boson mean-field theory which favors broken symmetry magnetic phases, our results suggest that the spin-liquid phase found here is robust against fluctuations. This spin liquid discussed in the following is most relevant to the spin-liquid candidate materials typically modeled through anisotropic triangular lattices with $J_2/J_1 > 1$ such as Cs_2CuCl_4 and Cs_2CuBr_4 for which the third-nearest-neighbor interactions are typically neglected.

This paper is organized as follows: In Sec. II, the $J_1-J_2-J_3$ Heisenberg model studied is introduced. In Sec. III, the Schwinger boson formulation is briefly revised and main issues described. In Sec. IV, the ground-state energies, magnetization, and phase diagram obtained with SB-MF are obtained and discussed. Elementary magnetic excitations of the system are discussed in Sec. V. We finally end up with conclusions and the relevance to anisotropic triangular lattice materials in Sec. VI.

II. HEISENBERG MODEL ON AN ANISOTROPIC TRIANGULAR LATTICE WITH THIRD-NEAREST-NEIGHBOR INTERACTIONS

We are interested in understanding the magnetic properties of the Heisenberg model on the anisotropic triangular lattice including exchanges up to third-nearest-neighbor spins:

$$H = J_1 \sum_{\langle ij \rangle} \mathbf{S}_i \cdot \mathbf{S}_j + J_2 \sum_{\langle\langle ij \rangle\rangle} \mathbf{S}_i \cdot \mathbf{S}_j + J_3 \sum_{\langle\langle\langle ij \rangle\rangle\rangle} \mathbf{S}_i \cdot \mathbf{S}_j. \quad (1)$$

We take from now on $J_1 = 1$ unless otherwise stated. The sum $\langle ij \rangle$ runs over nearest neighbors, $\langle\langle ij \rangle\rangle$ runs over next-nearest neighbors, and $\langle\langle\langle ij \rangle\rangle\rangle$ over third-nearest-neighbor pairs of sites. The model is illustrated in Fig. 1 on the lattice model topologically equivalent to the anisotropic triangular lattice including a third-nearest-neighbor interaction. We note that in the case of a third-nearest-neighbor exchange generated by ring exchange on a four-site plaquette, $J_3 \propto t_1^4/U^3$ and $J_3 \propto t_1^2 t_2^2/U^3$ for ring exchange on a rhombus (see [23] for more details). Our present model could also arise from direct exchange $J_3 \propto t_3^2/U$ through the hopping t_3 on a triangular lattice. The anisotropic triangular lattice model with no third-nearest neighbors $J_3 = 0$ has been studied extensively [10]. Related models including ring-exchange contributions also have been recently analyzed [23]. For the particular case of the isotropic triangular case, $J_2 = 1$ and $J_3 = 0$, Sachdev [11] finds a spin-liquid phase which becomes the long-range 120° magnetically ordered state when the quantum fluctuations are reduced to $S = 1/2$ within a Sp(N) formulation of the Heisenberg model where N is the number of spin species. The general $J_2 \neq 1$ situation has been explored using exact diagonalization and density-matrix renormalization group (DMRG) techniques [29], linear spin-wave theory (LSWT) [30,31], modified spin-wave theory [32], series expansions

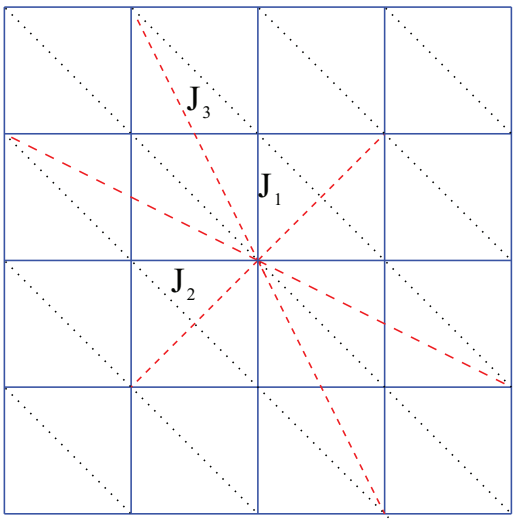

FIG. 1. (Color online) Picture of the $J_1-J_2-J_3$ Heisenberg model (1) considered. The lattice model studied has the same topology as the original anisotropic triangular lattice model in which each lattice site is connected to its nearest- (full blue lines), next-nearest- (dotted black lines), and third-nearest-neighbor sites (red dashed lines) through the antiferromagnetic exchange couplings J_1, J_2, and J_3, respectively.

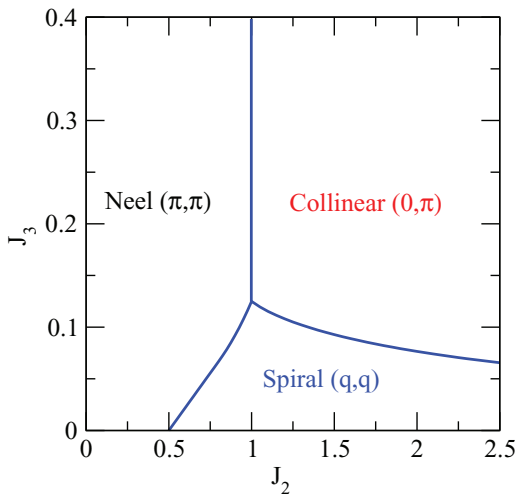

FIG. 2. (Color online) Classical phase diagram for the $J_1-J_2-J_3$ Heisenberg model (1) for the helical ground states. We have taken $J_1 = 1$.

[33], mean-field Schwinger boson theory [34], and large-N approaches [35]. In the region where a transition from Néel antiferromagnetism to spiral order occurs ($J_2 = 0.5$ within LSWT), a spin liquid has been speculated to exist. The isotropic triangular lattice model $J_2 = 1$ under the effect of J_3 has been studied [26] using Schwinger boson mean-field theory and recently revisited [21]. Spin-liquid phases have recently been found in the Hubbard model on the anisotropic triangular lattice [36].

Classical limit. The classical ground-state energy of model (1) is evaluated considering planar helices only. The spin at each site is given by $\mathbf{S_i} = S\cos(\mathbf{Q}\cdot\mathbf{R}_i)\mathbf{e_1} + S\sin(\mathbf{Q}\cdot\mathbf{R}_i)\mathbf{e_2}$, $\mathbf{e}_1$ and $\mathbf{e}_2$ being an orthonormal basis and $\mathbf{Q} = (Q_x, Q_y)$ the ordering wave vector. The classical phase diagram is obtained by comparing the energies of the spiral [$\mathbf{Q} = (Q,Q)$], collinear [$\mathbf{Q} = (0,\pi)/(\pi,0)$], and Néel [$\mathbf{Q} = (\pi,\pi)$] orders. The wave vector of the spiral phase is given by

$$Q = \arccos\left(\frac{-J_2 + \sqrt{J_2^2 + 12J_3(3J_3 - 1)}}{12J_3}\right). \quad (2)$$

The phase diagram resulting from these three phases is shown in Fig. 2. For $J_3 \to 0$, the transition between Néel and spiral order with $Q = \arccos(-1/2J_2)$ occurs at $J_2 = 0.5$ as expected for the anisotropic triangular lattice. In the isotropic limit, $J_2 = 1$, the transition from the spiral to collinear or Néel orders occurs at $J_3 = 0.125$. This is in agreement with the spin-wave analysis of model (1) on the isotropic triangular lattice: $J_1 = 1$, $J_2 = 1$, and $J_3 = 0$ [37].

III. SCHWINGER BOSON MEAN-FIELD THEORY

The quantum magnetism of bipartite (unfrustrated) lattices can be explored using the Schwinger bosonic representation of SU(N) Heisenberg models [25]. Extensions to frustrated lattices can be done by [38] using the Sp(N) representation. Here, we use the SU(2) mean-field theory introduced by Cecatto *et al.* [39] which keeps ferromagnetic and antiferromagnetic components in the mean-field approach. Such mean-field decoupling was found to correspond to the large-N limit of a "symplectic-N" representation of the spins [28] which appropriately takes into account time-reversal properties of the spins in frustrated magnets. The Schwinger boson approach can describe both magnetically ordered and disordered states complementing other semiclassical spin-wave theories. We now summarize the main steps in the Schwinger mean-field approach [25] to the Heisenberg model (1) following previous works [26–28,39–41].

Schwinger bosons are used to express the Heisenberg interaction terms in the model (1). Each bond between two different sites is expressed through the operator identity

$$\mathbf{S}_i \cdot \mathbf{S}_j = :\hat{B}_{ij}^\dagger \hat{B}_{ij}: - \hat{A}_{ij}^\dagger \hat{A}_{ij}, \quad (3)$$

where $: \ldots :$ is normal ordering, and the operators $\hat{A}_{ij}$ and $\hat{B}_{ij}$ are defined in terms of the Schwinger bosons as

$$\begin{aligned}\hat{A}_{ij} &= \tfrac{1}{2}(a_{i\uparrow}a_{j\downarrow} - a_{i\downarrow}a_{j\uparrow}),\\ \hat{B}_{ij} &= \tfrac{1}{2}(a_{i\uparrow}^\dagger a_{j\uparrow} + a_{i\downarrow}^\dagger a_{j\downarrow}),\end{aligned} \quad (4)$$

where $a_{i\uparrow}^\dagger$ and $a_{i\downarrow}^\dagger$ create a "spin-up" and "spin-down" Schwinger boson on site i. The two operators $\hat{A}_{ij}$ and $\hat{B}_{ij}$ describe antiferromagnetic and ferromagnetic bonds between i and j sites, respectively.

The magnitude of the spin is fixed by restricting the number of bosons per site:

$$\sum_\sigma a_{i\sigma}^\dagger a_{i\sigma} = 2S, \quad (5)$$

which is the constraint equation imposed over the Schwinger bosons avoiding having an arbitrary number of bosons at each site.

After a mean-field decoupling of the quartic terms describing the bonds, the Heisenberg model (1) can be expressed as a quadratic Hamiltonian:

$$\begin{aligned}H =\ & J_1 \sum_{\langle ij\rangle}(B_{ij}^*\hat{B}_{ij} - A_{ij}^*\hat{A}_{ij} + \text{H.c.})\\ &+ J_2 \sum_{\langle\langle ij\rangle\rangle}(B_{ij}^*\hat{B}_{ij} - A_{ij}^*\hat{A}_{ij} + \text{H.c.})\\ &+ J_3 \sum_{\langle\langle\langle ij\rangle\rangle\rangle}(B_{ij}^*\hat{B}_{ij} - A_{ij}^*\hat{A}_{ij} + \text{H.c.})\\ &+ J_1 \sum_{\langle ij\rangle}(-B_{ij}^*B_{ij} + A_{ij}^*A_{ij})\\ &+ J_2 \sum_{\langle\langle ij\rangle\rangle}(-B_{ij}^*B_{ij} + A_{ij}^*A_{ij})\\ &+ J_3 \sum_{\langle\langle\langle ij\rangle\rangle\rangle}(-B_{ij}^*B_{ij} + A_{ij}^*A_{ij})\\ &+ \lambda \sum_i \left(\sum_\sigma \langle a_{i\sigma}^+ a_{i\sigma}\rangle - 2S\right).\end{aligned} \quad (6)$$

The variational energy of the system is minimized with respect to A_{ij} and B_{ij} and the Lagrange multiplier λ fixes the constraint (5) at each site on average. The resulting set of self-consistent

equations obtained are

$$\begin{aligned}\langle \hat{A}_{ij}\rangle &= A_{ij},\\ \langle \hat{B}_{ij}\rangle &= B_{ij},\\ \sum_{\sigma}\langle a^{\dagger}_{i\sigma}a_{i\sigma}\rangle &= 2S,\end{aligned} \tag{7}$$

and the variational bond energy reads as

$$\langle \mathbf{S}_i\cdot\mathbf{S}_j\rangle = |B_{ij}|^2 - |A_{ij}|^2. \tag{8}$$

After Fourier transformation, the mean-field Hamiltonian reads

$$\begin{aligned}H^{\mathrm{MF}} = &\sum_{\mathbf{k},\sigma}[B(\mathbf{k})+\lambda]a^{\dagger}_{\mathbf{k},\sigma}a_{\mathbf{k},\sigma}\\ &- i\sum_{\mathbf{k}}A(\mathbf{k})(a_{\mathbf{k}\uparrow}a_{-\mathbf{k}\downarrow}+a^{\dagger}_{\mathbf{k}\uparrow}a^{\dagger}_{-\mathbf{k}\downarrow}) - 2\lambda N_s S,\end{aligned} \tag{9}$$

with N_s the number of sites in the lattice. The coefficients $A(\mathbf{k})$ and $B(\mathbf{k})$ are given by

$$\begin{aligned}A(\mathbf{k}) &= \frac{1}{2}\sum_{\boldsymbol{\delta}_i} J_i \sin(\mathbf{k}\cdot\boldsymbol{\delta}_i)A_{\boldsymbol{\delta}_i},\\ B(\mathbf{k}) &= \frac{1}{2}\sum_{\boldsymbol{\delta}_i} J_i \cos(\mathbf{k}\cdot\boldsymbol{\delta}_i)B_{\boldsymbol{\delta}_i},\end{aligned} \tag{10}$$

where the sums are performed over the $\boldsymbol{\delta}_i$ vectors connecting pairs of sites coupled by J_i; i.e., $\boldsymbol{\delta}_1$ refers to the vector connecting nearest-neighbor, $\boldsymbol{\delta}_2$ next-nearest-neighbor, and $\boldsymbol{\delta}_3$ third-nearest-neighbor sites. The variational parameters satisfy $A_{-\boldsymbol{\delta}_i} = -A_{\boldsymbol{\delta}_i}$ and $B_{-\boldsymbol{\delta}_i} = B_{\boldsymbol{\delta}_i}$, when evaluating the sums over $\boldsymbol{\delta}_i$.

A Bogoliubov transformation is performed to diagonalize the Hamiltonian. This leads to the following mean-field Hamiltonian:

$$H^{\mathrm{MF}} = \sum_{\mathbf{k},\sigma}\omega(\mathbf{k})\left(\alpha^{\dagger}_{\mathbf{k},\sigma}\alpha_{\mathbf{k},\sigma}+\frac{1}{2}\right) - N_s\lambda(1+2S), \tag{11}$$

where, for instance, the Bogoliubov spin-up quasiparticle is $\alpha^{\dagger}_{\mathbf{k},\uparrow} = \cosh(\theta_{\mathbf{k}})a^{\dagger}_{\mathbf{k},\uparrow} - \sinh(\theta_{\mathbf{k}})a_{-\mathbf{k}\downarrow}$, in terms of the original bosons with $\tanh(\theta_{\mathbf{k}}) = -\frac{A(\mathbf{k})}{B(\mathbf{k})+\lambda}$. Bogoliubov quasiparticles have the following dispersion:

$$\omega(\mathbf{k}) = \sqrt{[B(\mathbf{k})+\lambda]^2 - A(\mathbf{k})^2}. \tag{12}$$

From the minimization of the total energy $E_0 = \langle H^{\mathrm{MF}}\rangle$, a set of self-consistent equations

$$\begin{aligned}\frac{1}{2N_s}\sum_{\mathbf{k}}\frac{A(\mathbf{k})}{\omega(\mathbf{k})}\sin(\mathbf{k}\cdot\boldsymbol{\delta}_i) &= A_{\delta_i},\\ \frac{1}{2N_s}\sum_{\mathbf{k}}\frac{B(\mathbf{k})+\lambda}{\omega(\mathbf{k})}\cos(\mathbf{k}\cdot\boldsymbol{\delta}_i) &= B_{\delta_i},\\ \frac{1}{2N_s}\sum_{\mathbf{k}}\frac{B(\mathbf{k})+\lambda}{\omega(\mathbf{k})} &= \frac{1}{2}+S\end{aligned} \tag{13}$$

are obtained at zero temperature $T=0$, which are numerically solved. Extension to finite temperatures is discussed in Appendix B.

In a finite lattice with N_s sites, magnetic ordering with a particular order is signaled by a minimum gap in the spinon dispersion (located at $\pm\mathbf{Q}/2$) which scales as $\omega_{\pm\mathbf{Q}/2}\sim 1/N_s$, scaling to zero with the system size. In the thermodynamic limit, these modes go to zero and Bose condensation occurs at these wave vectors which signals a magnetically ordered state with ordering vector $\mathbf{Q}$. On infinite lattices, the sums in Eq. (13) are converted into integrals separating the macroscopic contribution of the condensed boson fraction at $\pm\mathbf{Q}/2$, which is treated as a self-consistent parameter $m(\mathbf{Q})$. The self-consistent equations (13) are solved under the extra condition $\omega_{\mathbf{Q}/2}=0$, which fixes $\lambda = A(\mathbf{Q}/2) - B(\mathbf{Q}/2)$ at each iteration $\mathbf{Q}$ is also obtained from minimization of the energy.

In large but finite systems, the magnetization can be obtained from [41]

$$m(\mathbf{Q}) = \frac{1}{N_s}\frac{B(\mathbf{Q}/2)+\lambda}{\omega(\mathbf{Q}/2)}. \tag{14}$$

We have checked that the magnetization $m(\mathbf{Q})$ and total energy E_0 converge to the thermodynamic limit results as the number of sites N_s is increased. One can show that the classical ground-state energy is recovered by SB-MF [26] in the $S\to\infty$ limit as it should (see Appendix A for details).

IV. GROUND-STATE PROPERTIES

We now analyze the ground-state properties of the Heisenberg model (1). We first discuss the phase diagram of the anisotropic triangular lattice and then the effect of the third-nearest-neighbor interactions J_3 on the phase diagram.

A. Anisotropic triangular lattice model ($J_3 = 0$)

It is illustrative to analyze first the ground-state properties of the anisotropic triangular lattice ($J_3 = 0$) with the SB-MF approach. In Fig. 3, we plot the J_2 dependence of magnetization and total energy. The magnetic wave vector $\mathbf{Q}$ changes continuously from (π,π) to (Q,Q) [34] at $J_2\approx 0.62$, which is larger than the classical transition point $J_2 = 0.5$ with no disordered phase found between Néel and spiral phases. Although the shift to higher J_2 critical values than the classical ones is consistent with series expansion [33] results, the SB-MF fails to describe the disordered region around $0.7 < J_2 < 0.9$ or the disordered phase at $J_2 = 0.5$ predicted by linear spin-wave theory (LSWT) [30,31]. On the other hand, increasing $J_2\approx 2.2$ a transition to a disordered state occurs consistent with the expected spin-liquid phase in decoupled $S=\frac{1}{2}$ spin chains ($J_1 = 0$). Note that this critical SB-MF value is much smaller than $J_2\approx 3.8$ from LSWT [30,31] or series expansions $J_2\approx 4.5$ [33].

B. Effect of third-nearest-neighbor interactions ($J_3 \neq 0$)

We now analyze the effect of the third-nearest-neighbor interaction. Results for the total energy per site and magnetization dependence on J_3 are shown in Fig. 4 for different J_2.

The isotropic triangular lattice case has been previously studied [26] with Schwinger bosons and recently revisited [21]. A first-order transition from 120° Néel ordering [$\mathbf{Q} = (2\pi/3, 2\pi/3)$] to collinear order with $\mathbf{Q} = (0,\pi)$ occurs at about $J_3\approx 0.16$. These values should be compared with the classical spin-wave [37] values with the spiral-collinear

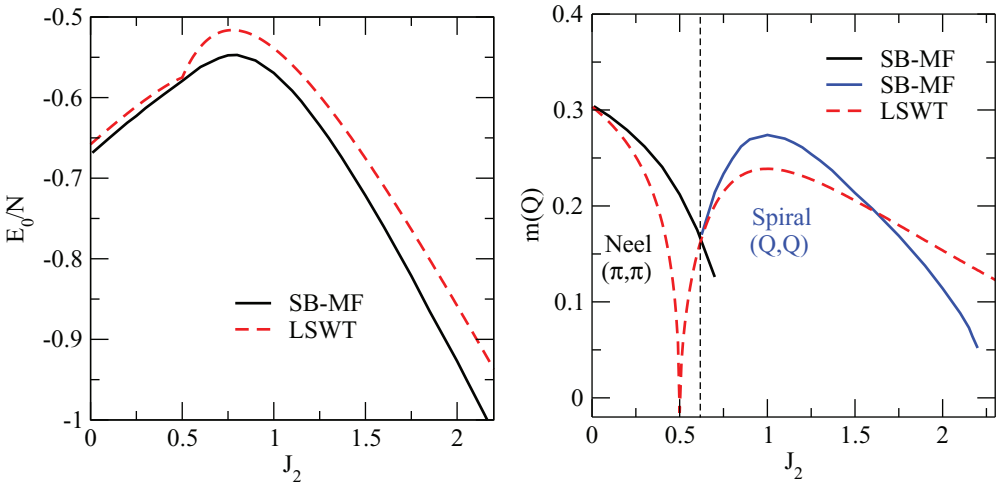

FIG. 3. (Color online) Ground-state properties of the anisotropic triangular lattice. The ground-state energy (left) and magnetization (right) of model (1) with $J_3 = 0$ are shown. Dependence of ground-state energy E_0 and magnetization $m(\mathbf{Q})$, with J_2 from Schwinger boson mean-field theory. Schwinger boson mean-field theory does not show a disordered spin-liquid phase between the Néel and spiral phases in contrast to spin-wave theory (dashed lines) at $J_2 = 0.5$. A spin-liquid phase occurs in SB-MF for $J_2 > 2.2$, a much smaller value than that obtained from series expansions or LSWT. The dotted vertical line marks the onset of the continuous direct transition from the Néel to the spiral phase in SB-MF for $J_2 \approx 0.63$ [34].

transition occurring at $J_3 = 0.125$. The direct spiral-collinear transition survives up to $J_2 \gtrsim 1.8$, at which a disordered spin liquid is stabilized between the (Q,Q)-spiral and $(0,\pi)$-collinear order.

The dependence of the ordering wave vector $\mathbf{Q}$ with J_3 is shown in Fig. 5 for different J_2. The absolute value of Q in $\mathbf{Q} = (Q,Q)$ is plotted as a function of J_3 until the jump to the $(0,\pi)$ phase occurs showing the discontinuous behavior of the order parameter signaling the first-order transition. For comparison, we plot the dependence of the classical ordering wave vector as a function of J_3 showing how the transition point $(J_3)_c$ is shifted to larger values by the quantum fluctuation effects. Also, it shows how the SB-MF ordering vector is enhanced with respect to the classical ordering vector for $J_2 < 1$ and is reduced when $J_2 > 1$ independent of the value of J_3. For $J_2 = 1$, the SB-MF ordering vector $Q = 2\pi/3$ is identical to the classical wave vector. Our results extend previous studies for the anisotropic triangular case with $J_3 = 0$.

We summarize the results of ground-state properties of the $J_1-J_2-J_3$ model of Fig. 5 in which the SB-MF phase diagram is compared with the classical phase diagram in Fig. 2.

V. MAGNETIC EXCITATIONS

We now discuss the elementary excitations of the system in different parameter regimes. Magnetically ordered states can be described with the infinite lattice version of the SB-MF with

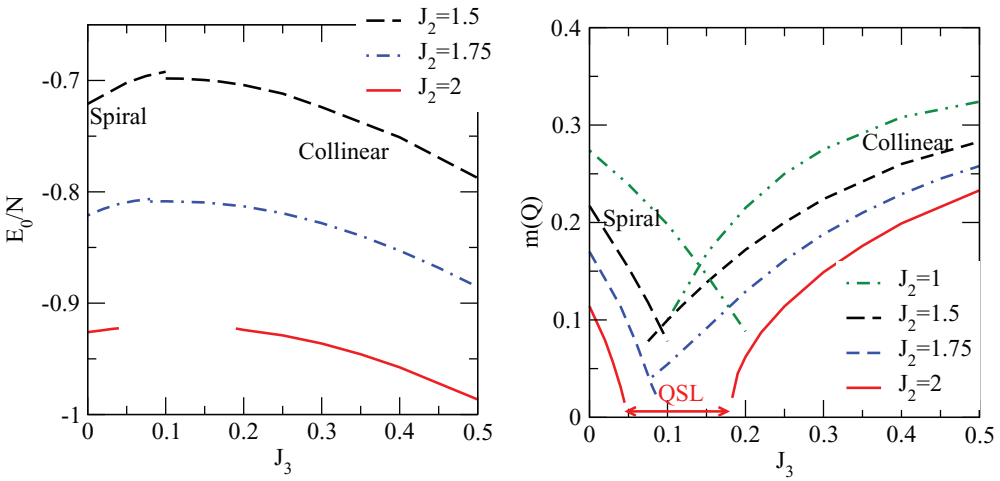

FIG. 4. (Color online) Spin-liquid phase in the $J_1-J_2-J_3$ Heisenberg model on the anisotropic triangular lattice. The dependence of magnetization and energy on the third-nearest-neighbor interaction J_3 from Schwinger boson mean-field theory in infinite lattices. The energy curves are broken in the region where no magnetically ordered solution is found. A spin-liquid (QSL) phase occurs between the spiral-(Q,Q) and collinear-$(0,\pi)$ phases for $J_2 \gtrsim 1.8$ for a small $J_3 < 0.1$.

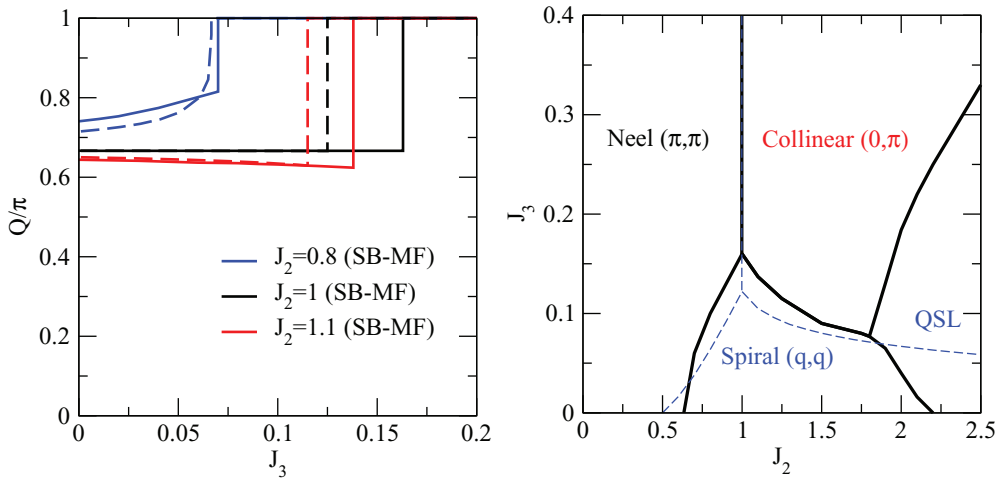

FIG. 5. (Color online) Ordering wave vector and Schwinger boson mean-field phase diagram of the $J_1-J_2-J_3$ model on an anisotropic triangular lattice. In the left panel, the dependence of $\mathbf{Q}$ on J_3 showing the transition from the spiral-(Q,Q) to the collinear-$(0,\pi)$ phase for which we set $Q=\pi$ for the purposes of this figure from SB-MF (solid lines) is compared to the classical wave-vector dependence. The ground-state phase diagram obtained from SB-MF (solid lines) is compared with the classical phase diagram (dashed lines) in the right panel showing the parameter range in which the spin-liquid phase (QSL) is stable.

the extra condition $\omega(\pm\mathbf{Q}/2)=0$. These types of solutions are recovered in large but finite lattices by using Eq. (B1) with no extra condition. These solutions do not break the spin symmetry but have dispersions with a minimum energy which behaves as $\omega(\pm\mathbf{Q}/2)\propto 1/N_s$. Disordered phases preserving the SU(2) spin symmetry of the Hamiltonian are described through the version of the SB-MF approach expressed in Eq. (B1).

A. Elementary excitations: One-spinon dispersions

The elementary excitations in the spin-liquid phase described through SB-MF are the $S=1/2$ spinons. These can be visualized within Anderson "resonant valence bond" (RVB) theory as $S=1/2$ defects propagating in the background of resonating singlets covering the rest of the lattice. The SB-MF theory presented here including singlet A_{ij} and triplet B_{ij} correlations corresponds to a large-N saddle point [28] which appropriately deals with the time-reversal properties of the spin in contrast to previous Sp(N) theories [11]. At the large-N saddle point or the SB-MF theory (for $N=2$) presented here, spinons are noninteracting.

The evolution of the one-spinon dispersion starting from the ordered (Q,Q) spiral phase as J_3 is increased with $J_2=2$ is shown in Fig. 6. Initially when $J_2=0$, the spinon dispersion is gapless and the spinons are Bose condensed at the $\pm\mathbf{Q}/2$ wave vectors leading to a small but finite magnetization. As J_3 is increased and the disordered spin liquid reached the spinon dispersion develops a gap at $\pm\mathbf{Q}/2$ and long-range order is lost.

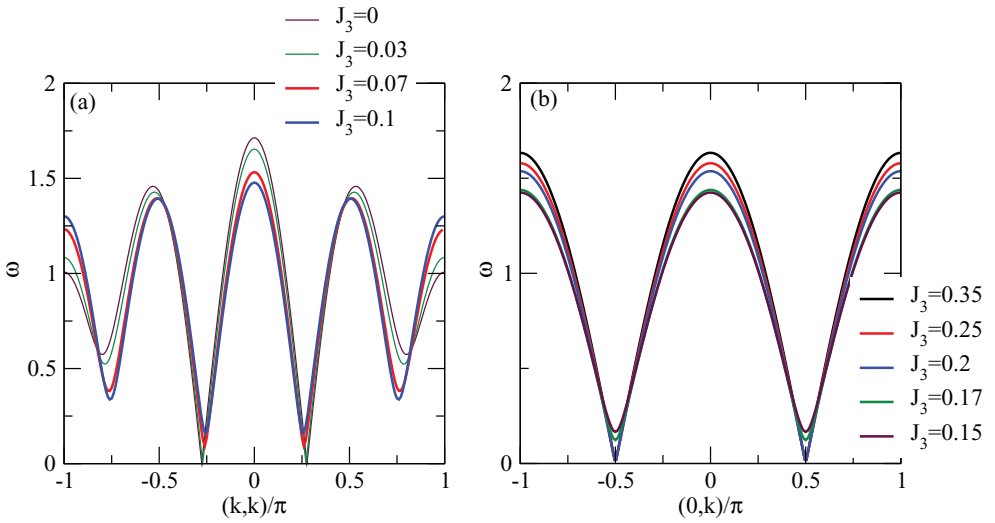

FIG. 6. (Color online) Spinon dispersion for the $J_1-J_2-J_3$ model with $J_2=2$ and various J_3. In (a) we show the evolution of the spinon dispersion along the diagonal (k,k) direction of the Brillouin zone from the magnetically ordered spiral-(Q,Q) phase to the spin-liquid phase. In (b) the evolution of the spinon dispersion in the $(0,k)$ direction from the collinear $(0,\pi)$ to the spin liquid is shown. The spin-liquid phases are characterized by the opening of a gap.

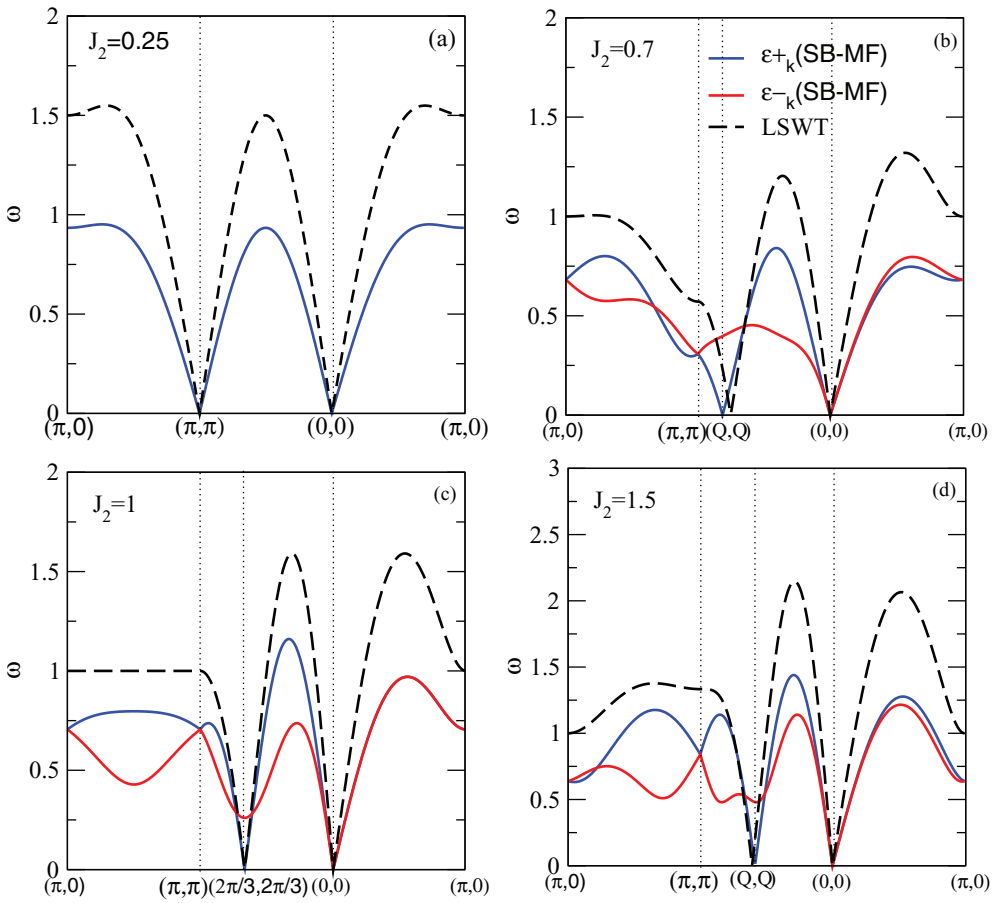

FIG. 7. (Color online) Evolution of lowest two-spinon continuum energies from Schwinger boson mean-field theory on an anisotropic triangular lattice ($J_3 = 0$). The blue and red full lines correspond to the $\epsilon_{\mathbf{k}\pm\mathbf{Q}/2}$, in Eq. (15), respectively. We show results within the (a) Néel phase with $J_2 = 0.25$, (b) spiral state with $J_2 = 0.7$, (c) isotropic triangular lattice, and (d) $J_2 = 1.5$. All these cases correspond to magnetically ordered phases. The LSWT magnon dispersions are shown for comparison (dashed lines). Note that in the Néel phase the $\epsilon_{\mathbf{k}\pm\mathbf{Q}/2}$ excitations coincide.

The evolution of the spinon dispersions starting from the collinear-$(0,\pi)$ phase is also shown in Fig. 6 showing how the the gap opens at $(0, \pm\pi/2)$ on entering the spin-liquid phase.

B. Two-spinon excitations

The $S = 1/2$ Heisenberg antiferromagnetic chain with nearest-neighbor interaction J has no long-range magnetic order and no energy gap to the lowest excitation dispersion [42] $\omega_q = \frac{\pi J}{2}|\sin q|$. Hence, magnetic excitations consist of a two-spinon continuum different from the well-defined dispersion of magnons, the magnetic quasiparticles expected in a three-dimensional ordered Heisenberg antiferromagnet.

Within SB-MF, the triplet excitations can be formed by the composition of two spin-1/2 deconfined spinons. These form a broad particle-hole continuum which reaches high energies with the minimum excitation energy related to magnetic order in ordered phases. In an ordered phase, the lowest magnetic excitations are obtained by creating a spinon in the condensate and another spinon in the continuum. The minimum two-spinon excitation energies read as

$$\epsilon^{\pm}_{\mathbf{k}} = \omega(\mp\mathbf{Q}/2) + \omega(\mathbf{k} \pm \mathbf{Q}/2), \qquad (15)$$

where $\omega(\mp\mathbf{Q}/2) \to 0$, and $\epsilon^{\pm}_{\mathbf{k}} = \omega(\mathbf{k} \pm \mathbf{Q}/2)$ in an ordered phase.

In Fig. 7, we show the minimum two-spinon excitation energies of the continuum $\epsilon^{\pm}_{\mathbf{k}}$ as obtained from Eq. (15) on an anisotropic triangular lattice ($J_3 = 0$). This is plotted in Fig. 7 for different J_2 and compared to magnons obtained from spin-wave theory. We show the evolution of these dispersions when going from the Néel to the spiral phases including the isotropic triangular lattice case already discussed in the literature [41].

(i) *Néel phases.* In the Néel phases, we find that the lowest SB-MF dispersions are very similar to the conventional magnon excitations. This is shown in Fig. 7(a) for $J_2 = 0.25$. The only important effect is the smaller width of the SB-MF dispersions as compared to the semiclassical LSWT dispersion. This is due to renormalization effects since the SB-MF theory contains static interaction effects [25] in a similar way as Hartree-Fock theory contains band renormalization and band shift effects in interacting electron models. Series expansion calculations in this regime have found the development of "roton" minima [43] around $(\pi,0)$ in the $(\pi,0) \to (\pi/2,\pi/2)$ direction with a lower energy at $(\pi,0)$ with respect to the $(\pi/2,\pi/2)$ wave vector. Both LSWT and SB-MF disagree with the series expansion results, which predict a flat dispersion (not shown) between these wave vectors. A simple interpretation in terms of noninteracting spinons for these roton minima does not seem adequate and one may need

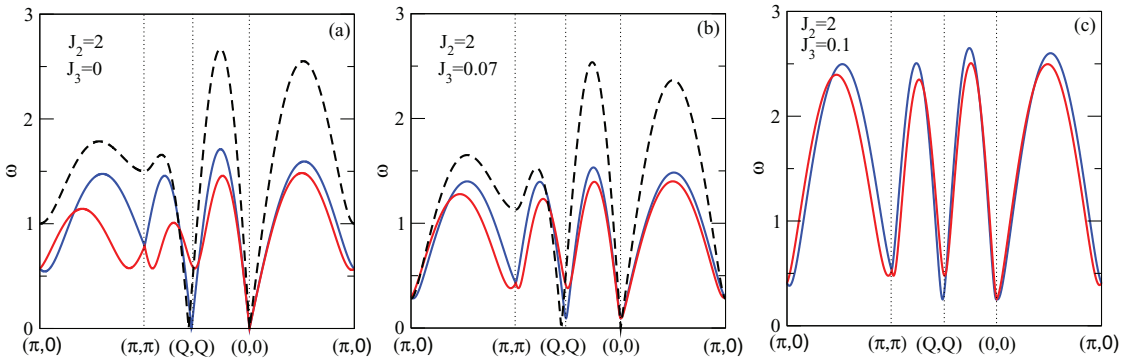

FIG. 8. (Color online) Evolution of the lowest energies of the two-spinon continuum from Schwinger boson mean-field theory on the $J_1-J_2-J_3$ for $J_2 = 2$ and different J_3. The plots and labels are the same as in Fig. 7. In (a) for $J_3 = 0$, the system is in an ordered spiral phase whereas in (b) for $J_2 = 0.07$, the system is a spin-liquid state characterized by a small energy gap ~ 0.1 and short-range spiral (Q,Q) correlations. In (c) the same plots for $J_3 = 0.1$ showing the enhancement of the gap.

to go beyond the mean-field theory and include spinon-spinon interactions.

(ii) *Spiral phases.* When entering the spiral phase we find the strongest deviations of the dispersions with respect to the LSWT. Already for $J_2 = 0.7$ [Fig. 7(b)] we find that apart from the renormalization effects discussed above there are also qualitative differences in the momentum dependence in the $(\pi,0)$-(π,π) direction. In the isotropic triangular case, there is a flat band dispersion between $(\pi,0) \rightarrow (\pi,\pi)$ in LSWT which is not observed in the SB-MF dispersion but rather a minimum (maximum) occurs in the lowest (highest) branch at $(\pi,\pi/2)$ and dips at the (π,π) and $(\pi,0)$ points which compare well with the roton minima observed in the series expansion results [27]. This minima can be associated with the existence of (π,π)-Néel and $(0,\pi)[/(\pi,0)]$-collinear correlations [41] in the (Q,Q)-spiral ordered phase. For larger J_2, the differences with the spin-wave dispersion become more pronounced particularly around (π,π) where a deeper dip is observed compared to the LSWT magnon dispersions as in Fig. 7(d).

(iii) *Spin-liquid formation.* We now discuss the evolution in the large-J_2 limit where a spin-liquid phase occurs. In Fig. 8, we fix $J_2 = 2$ and increase J_3 so that we eventually enter the spin-liquid phase. For $J_3 \gtrsim 0.05$, the system enters the spin-liquid phase and a small gap opens in the dispersion around the short-range ordering spiral vector (Q,Q). Concomitantly, there is a change in the momentum dependence of the dispersion with suppression of the dispersion at $(\pi,0)$ as compared to the $J_3 = 0$ case which indicates the proximity to the collinear phase. This is consistent with the expected behavior as extracted from the phase diagram (see Fig. 5). We also show in Fig. 8 the spin liquid obtained for $J_3 = 0.1$.

The above low-energy magnetic dispersions will be modified in general in the presence of finite-N fluctuations around the saddle point. These generate gauge interactions that bind the spinons which in the ordered phases lead to magnons in the neighborhood of the Goldstone modes. On the other hand, at high energy, pairs of spinons remain weakly bound.

C. Dynamical magnetic correlations

The dynamics of the spin correlations in the system can be analyzed through inelastic magnetic neutron scattering experiments which probe the $\Delta S = \pm 1$ excitations. If there are magnons present in the magnetic excitation spectra, as in conventional magnets, then sharp quasiparticle peaks are found in the neutron scattering spectra. Since spinons carry half of the local spin degree of freedom at each lattice site $\Delta S = \pm 1$, magnetic excitations observed in neutron scattering can occur from the triplet combination of two spinons. Within SB-MF, spinons are deconfined leading to a two-spinon continuum rather than the sharp magnon quasiparticle peaks of conventional magnets. The dynamical spin correlation function obtained in the SB-MF then reads as

$$S^{zz}(\mathbf{k},\omega) = \sum_n \left|\langle 0|S^z_{\mathbf{k}}|n\rangle\right|^2 \delta[\omega - (E_n - E_0)], \qquad (16)$$

with $S^z_{\mathbf{k}} = \frac{1}{N_s}\sum_i e^{i\mathbf{k}\cdot\mathbf{R}_i} S^z_i$ and $S^z_i = \frac{1}{2}(a^\dagger_{i\uparrow}a_{i\uparrow} - a^\dagger_{i\downarrow}a_{i\downarrow})$. We evaluate this expression at the mean-field level using the Schwinger boson approach. The ground state is defined as the vacuum of Bogoliubov quasiparticles: $\alpha_{\mathbf{k}\sigma}|0\rangle = 0$ where $\alpha_{\mathbf{k}\sigma}$ destroys a Bogoliubov quasiparticle for any $\mathbf{k}$ and σ as in Eq. (11). Excitation n is produced by creating two spinons above the vacuum.

Expressing the original boson operators in terms of the Bogoliubov quasiparticles with the two-spinon excitations $E_n - E_{\mathrm{GS}} = \omega(\mathbf{k_1}) + \omega{-}(\mathbf{q}+\mathbf{k_1})$, the final expression for the spin correlation function reads as

$$S^{zz}(\mathbf{k},\omega) = \frac{1}{4N_s}\sum_{\mathbf{k_1}} \left|u_{\mathbf{k}+\mathbf{k_1}} v_{\mathbf{k_1}} - u_{\mathbf{k_1}} v_{\mathbf{k}+\mathbf{k_1}}\right|^2 \times \delta\big[\omega - \big(\omega(-\mathbf{k_1}) + \omega(\mathbf{k}+\mathbf{k_1})\big)\big], \qquad (17)$$

with the matrix elements $u_{\mathbf{k}} = \sqrt{(1 + \frac{B(\mathbf{k})+\lambda}{\omega(\mathbf{k})})/2}$ and $v_{\mathbf{k}} = i\,\mathrm{sign}[A(\mathbf{k})]\sqrt{(-1 + \frac{B(\mathbf{k})+\lambda}{\omega(\mathbf{k})})/2}$. The above Eq. (17) gives the spectra of $S = 1$ excitations relevant to neutron scattering consisting on two spinons. The lowest-energy particle-hole processes described by $S^{zz}(\mathbf{k},\omega)$ correspond to exciting a spinon from the condensate and another one from the continuum. For finite-size lattices, $[B(\mathbf{Q}) + \lambda]/\omega(\mathbf{Q}/2) = N_s m(\mathbf{Q})$, $u_{\pm\mathbf{Q}/2} \sim \sqrt{N_s m(\mathbf{Q})/2}$, and $v_{\pm\mathbf{Q}/2} \sim i\sqrt{N_s m(\mathbf{Q})/2}$ and so the weight right at $\pm\mathbf{Q}/2$ is proportional to the magnetization.

In Fig. 9, the dynamical spin correlations $S^{zz}(\mathbf{k},\omega)$ are shown for $J_2 = 2$ going from the spiral ordered phase into

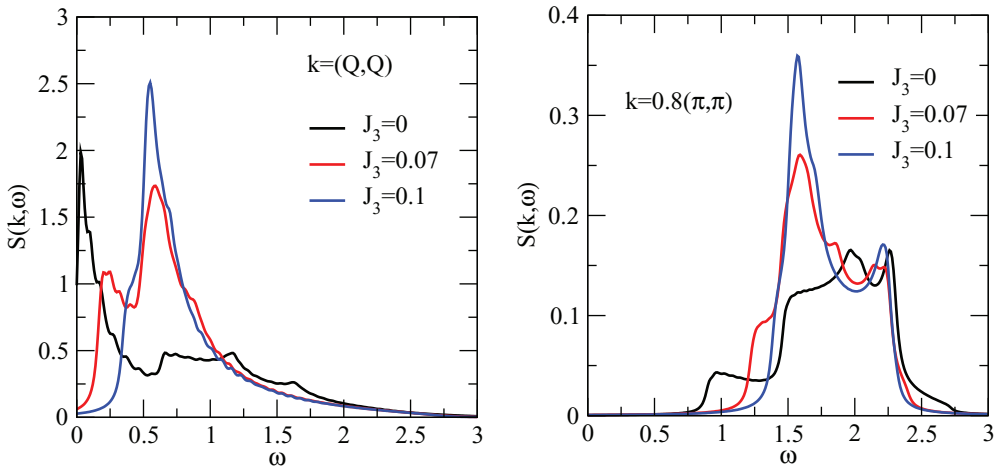

FIG. 9. (Color online) Dynamical spin structure factor $S^{zz}(\mathbf{k},\omega)$ for $J_2 = 2$. In the left panel we show $S^{zz}(\mathbf{k},\omega)$ at the spiral ordering wave vector $\mathbf{Q}$, whereas in the right panel we use $\mathbf{k} = 0.8(\pi,\pi)$. The plot shows how the two-spinon continuum described by Schwinger boson mean-field theory reaches high energies of about 2.5–3 which is an artifact of the approach [41]. Note the much smaller vertical scale in the right plot, i.e., away from the ordering wave vector $\mathbf{Q}$.

the spin-liquid phase corresponding to parameters shown in Fig. 8. The main features observed in the spectra correspond to the elementary two-spinon branches $\epsilon^{\pm}_{\mathbf{k}}$ plotted in Fig. 8. We first concentrate in $S(\mathbf{k},\omega)$, evaluated at the ordering wave vector $\mathbf{Q} = (Q,Q)$. In the ordered phase for $J_3 = 0$, there is a very low-energy peak (going to zero in the infinite system) which dominates the spectra and corresponds to the Goldstone mode associated with the long-range spiral magnetic order. A second smaller feature occurs at the second elementary branch of Fig. 8. Apart from these two main features, there is a contribution of particle-hole excitations which extends up to high energies. Such contribution is associated with two-spinon excitation processes involving spinons in the normal fluid (not condensed) as recently pointed out [41]. As J_3 is increased, there is a redistribution of spectral weight. On entering the spin-liquid phase, a gap opens up in the spectra and the spectral weight of the lowest branch is suppressed while there is an enhancement of spectral weight of the highest magnetic excitation. For the wave vector $\mathbf{k} = 0.8(\pi,\pi)$ different from $\mathbf{Q}$, there is also a two-peak structure similar to the one discussed above associated with $\epsilon^{\pm}_{\mathbf{k}}$. However, the overall spectral weight contribution is suppressed as compared to $\mathbf{Q} = (Q,Q)$ since excitations have higher energy.

VI. CONCLUSIONS

We have analyzed the effect of a third-nearest-neighbor antiferromagnetic interaction J_3 on the magnetic properties of the antiferromagnetic Heisenberg model on an anisotropic triangular lattice. We have shown that J_3 can frustrate the long-range spiral magnetic order leading to a spin-liquid phase when $J_2 > 1.8$ and a small $J_3 \lesssim 0.1$. Since SB-MF is known to favor ordered states [25], the parameter regime in which the spin-liquid phase is stable may be enlarged by fluctuations.

The antiferromagnetic coupling J_3 considered here may be generated through either second-order, superexchange processes between third-nearest-neighbor sites or fourth-order processes, that also drive ring exchange. Ring exchange involving four sites can be separated into two-spin J_3 Heisenberg and four-spin [22,23] contributions. Our present analysis, focusing on the frustrating effects associated with the former Heisenberg-type exchange terms in the ring exchange, is helpful in the understanding of ring-exchange effects in frustrated antiferromagnets.

Our analysis may be relevant to recent observations suggesting spin-liquid behavior in certain layered materials. Cs_2CuBr_4 is an anisotropic triangular material with $J_2 \sim 2$ which would be predicted to be magnetically ordered. However, from our analysis, a rather small J_3 would be sufficient to turn it into a spin liquid. On the other hand, Cs_2CuCl_4 with $J_2 \sim 3$ would be a spin liquid from our analysis even for $J_3 = 0$ which is in contrast with series expansion predictions. In any case, our SB-MF analysis suggests that in these two materials J_3 may play a role in determining their magnetic properties [17]. On the other hand, organic materials in which spin-liquid phases have been found such as κ-(BEDT-TTF)$_2$Cu$_2$(CN)$_3$ and Me$_3$EtSb[Pd(dmit)$_2$]$_2$ are in a different parameter regime $J_2 \sim 0.7$ in which SB-MF would predict an ordered state regardless of J_3 unlike the spin liquid predicted by series expansions [33] for $J_3 = 0$. On the basis of this work, one would expect a finite J_3 to further stabilize the QSL. It would be interesting to find organic materials which are in the large-J_2 parameter regime discussed here as they would be strong candidates for the observation of spin-liquid behavior.

The SB-MF prediction for the magnetically disordered state is a Z_2 spin liquid [11,44] characterized by gapped bosonic excitations. However, the T dependence of the NMR relaxation rate in Cs_2CuCl_4 and κ-(BEDT-TTF)$_2$Cu$_2$(CN)$_3$ suggests the presence of gapless excitations in the system. This fact can be more naturally explained in terms of fermionic mean-field theories with a ground state consisting of a spinon Fermi surface [12] but is also not inconsistent with a gap smaller [15] than $0.1J_1$. Further theoretical efforts should concentrate in understanding these observations by going beyond the mean-field theory used here using numerical

techniques that can treat the constraint on the number of bosons exactly.

ACKNOWLEDGMENTS

This work was funded in part by the Australian Research Council under the Discovery (Grant No. DP1093224), Future (Grant No. FT130100161), and QEII (Grant No. DP0878523) schemes. J.M. acknowledges financial support from MINECO (Grant No. MAT2012-37263-C02-01).

APPENDIX A: CLASSICAL ENERGY

Here, we analyze how in the $S \to \infty$ limit the ground-state energy obtained from SB-MF converges to the classical ground-state energy [26]. Self-consistent solutions of the bond strengths of the model in the classical limit are given by

$$B_{ij} \approx S\cos(\mathbf{Q}\cdot\mathbf{R}_{ij}/2),$$
$$A_{ij} \approx S\sin(\mathbf{Q}\cdot\mathbf{R}_{ij}/2), \tag{A1}$$

where $\mathbf{R}_{ij}$ is the distance between two sites forming a bond. One can check that the classical energy for a given bond is indeed recovered:

$$\langle \mathbf{S}_i\cdot\mathbf{S}_j\rangle = |B_{ij}|^2 - |A_{ij}|^2 \approx S^2\cos(\mathbf{Q}\cdot\mathbf{R}_{ij}). \tag{A2}$$

The boson chemical potential in the magnetically ordered phase is then given by

$$\lambda = A(\mathbf{Q}/2) - B(\mathbf{Q}/2) = -SJ(\mathbf{Q}) = -\frac{E_{\text{class}}}{S}, \tag{A3}$$

where we have defined

$$\begin{aligned} J(\mathbf{Q}) = {} & J_1[\cos(Q_x)+\cos(Q_y)] + J_2\cos(Q_x+Q_y) \\ & + J_3[\cos(Q_x-Q_y)+\cos(2Q_x+Q_y) \\ & + \cos(Q_x+2Q_y)], \end{aligned} \tag{A4}$$

and the classical energy $E_{\text{class}} = S^2 J(\mathbf{Q})$. The mean-field energy per site referred to the chemical potential obtained from H^{MF} reads as

$$E = \langle H^{\text{MF}}\rangle + 2\lambda S = \frac{1}{N_s}\sum_{\mathbf{k}}\omega(\mathbf{k}) + S^2 J(\mathbf{Q}) \approx E_{\text{class}}, \tag{A5}$$

when S is large since the sum over $\omega(\mathbf{k})$ in the right-hand side of the equation is of $O(S)$ only. Therefore, when $S \to \infty$, the SB-MF energy converges to the classical energy.

APPENDIX B: FINITE-TEMPERATURE EFFECTS

We finally comment on finite-temperature effects. The SB-MF approach can be extended trivially to finite temperatures by minimizing the total free energy of the system leading to the set of self-consistent equations [27]

$$\begin{aligned} \frac{1}{2N_s}\sum_{\mathbf{k}}\frac{A(\mathbf{k})}{\omega(\mathbf{k})}\{1+2n(\omega(\mathbf{k}))\}\sin(\mathbf{k}\cdot\boldsymbol{\delta}_i) &= A_{\delta_i}, \\ \frac{1}{2N_s}\sum_{\mathbf{k}}\frac{B(\mathbf{k})+\lambda}{\omega(\mathbf{k})}\{1+2n(\omega(\mathbf{k}))\}\cos(\mathbf{k}\cdot\boldsymbol{\delta}_i) &= B_{\delta_i}, \\ \frac{1}{2N_s}\sum_{\mathbf{k}}\frac{B(\mathbf{k})+\lambda}{\omega(\mathbf{k})}\{1+2n(\omega(\mathbf{k}))\} &= \frac{1}{2}+S, \end{aligned} \tag{B1}$$

where $n(\omega) = \frac{1}{e^{\beta\omega}-1}$, the Bose function and $\beta = 1/T$. The above equations are numerically solved at any given temperature. We have obtained the temperature dependence of the gap in the excitation spectrum within the spin-liquid phase. We find that the gap $\Delta(T)$ increases with temperature. Since the spin-correlation length $\xi \propto 1/\Delta(T)$, this means that the correlation length is suppressed with temperature as it should. The SB-MF approach can describe spin-liquid states with short-range spin correlations. However, at temperatures $T \gtrsim 0.4J$, we find that variational parameters A_δ, B_δ vanish (see also [27]). This indicates that SB-MF is unable to describe paramagnetic phases occurring, for instance, in the experimental phase diagram of Cs_2CuCl_4. This is in contrast to recent work using a spin representation based on Majorana fermions [45] which consistently describes the transition line from the spin-liquid to the paramagnetic phase. Further work which goes beyond the mean-field treatment presented here is needed to describe paramagnetic phases stabilized by temperature.

[1] L. Balents, Nature (London) **464**, 199 (2010).
[2] N. Ashcroft and D. Mermin, *Solid State Physics* (Thomson-Learning, Stamford, CT, 1975).
[3] A. Tsvelik, *Quantum Field Theory in Condensed Matter Physics* (Cambridge University Press, Cambridge, UK, 2003).
[4] C. Janani, J. Merino, I. P. McCulloch, and B. J. Powell, arXiv:1401.6605.
[5] E. P. Scriven and B. J. Powell, Phys. Rev. Lett. **109**, 097206 (2012).
[6] J. O. Fjærestad, W. Zheng, R. R. P. Singh, R. H. McKenzie, and R. Coldea, Phys. Rev. B **75**, 174447 (2007).
[7] Y. Shirata, H. Tanaka, A. Matsuo, and K. Kindo, Phys. Rev. Lett. **108**, 057205 (2012).
[8] H. D. Zhou, E. S. Choi, G. Li, L. Balicas, C. R. Wiebe, Y. Qiu, J. R. D. Copley, and J. S. Gardner, Phys. Rev. Lett. **106**, 147204 (2011).
[9] T. Susuki, N. Kurita, T. Tanaka, H. Nojiri, A. Matsuo, K. Kindo, and H. Tanaka, Phys. Rev. Lett. **110**, 267201 (2013).
[10] B. J. Powell and R. H. McKenzie, Rep. Prog. Phys. **74**, 056501 (2011).
[11] S. Sachdev, Phys. Rev. B **45**, 12377 (1992).
[12] O. I. Motrunich, Phys. Rev. B **72**, 045105 (2005).
[13] Y. Shimizu, K. Miyagawa, K. Kanoda, M. Maesato, and G. Saito, Phys. Rev. B **73**, 140407 (2006).
[14] B. Normand, Contemp. Phys. **50**, 533 (2009).
[15] M.-A. Vachon *et al.*, New J. Phys. **13**, 093029 (2011).
[16] M. Kohno, O. A. Starykh, and L. Balents, Nat. Phys. **3**, 790 (2007).
[17] R. Coldea, D. A. Tennant, A. M. Tsvelik, and Z. Tylczynski, Phys. Rev. Lett. **86**, 1335 (2001); R. Coldea, D. A. Tennant, and Z. Tylczynski, Phys. Rev. B **68**, 134424 (2003).

[18] N. Elstner, R. R. P. Singh, and A. P. Young, Phys. Rev. Lett. **71**, 1629 (1993).
[19] B. Bernu, P. Lecheminant, C. Lhuillier, and L. Pierre, Phys. Rev. B **50**, 10048 (1994).
[20] P. W. Anderson, Mater. Res. Bull. **8**, 153 (1973).
[21] F. Wang and A. Vishwanath, Phys. Rev. B **74**, 174423 (2006).
[22] W. LiMing, G. Misguich, P. Sindzingre, and C. Lhuillier, Phys. Rev. B **62**, 6372 (2000); G. Misguich, C. Lhuillier, B. Bernu, and C. Waldtmann, *ibid.* **60**, 1064 (1999).
[23] M. Holt, B. J. Powell, and J. Merino, Phys. Rev. B **89**, 174415 (2014).
[24] L. Messio, O. Cépas, and C. Lhuillier, Phys. Rev. B **81**, 064428 (2010).
[25] A. Auerbach, *Interacting Electrons and Quantum Magnetism* (Springer, Berlin, 1994).
[26] C. J. Gazza and H. A. Ceccatto, J. Phys: Condens. Matter **5**, L135 (1993).
[27] A. Mezio, L. O. Manuel, R. R. P. Singh, and A. E. Trumper, New J. Phys. **14**, 123033 (2012).
[28] R. Flint and P. Coleman, Phys. Rev. B **79**, 014424 (2009).
[29] M. Q. Weng, D. N. Sheng, Z. Y. Weng, and R. J. Bursill, Phys. Rev. B **74**, 012407 (2006).
[30] A. E. Trumper, Phys. Rev. B **60**, 2987 (1999).
[31] J. Merino, R. H. McKenzie, J. B. Marston, and C. H. Chung, J. Phys.: Condens. Matter **11**, 2965 (1999).
[32] P. Hauke, Phys. Rev. B **87**, 014415 (2013).
[33] Z. Weihong, R. H. McKenzie, and R. R. P. Singh, Phys. Rev. B **59**, 14367 (1999).
[34] L. O. Manuel and H. A. Ceccatto, Phys. Rev. B **60**, 9489 (1999).
[35] C. H. Chung, J. B. Marston, and Ross H. McKenzie, J. Phys.: Condens. Matter **13**, 5159 (2001).
[36] L. F. Tocchio, H. Feldner, F. Becca, R. Valentí, and C. Gros, Phys. Rev. B **87**, 035143 (2013).
[37] Th. Jolicoeur, E. Dagotto, E. Gagliano, and S. Bacci, Phys. Rev. B **42**, 4800 (1990).
[38] N. Read and S. Sachdev, Phys. Rev. Lett. **66**, 1773 (1991).
[39] H. A. Ceccatto, C. J. Gazza, and A. E. Trumper, Phys. Rev. B **47**, 12329 (1993).
[40] K. Lefmann and P. Hedegard, Phys. Rev. B **50**, 1074 (1994).
[41] A. Mezio *et al.*, Europhys. Lett. **94**, 47001 (2011).
[42] J. des Cloizeaux and J. J. Pearson, Phys. Rev. **128**, 2131 (1962).
[43] W. Zheng, J. O. Fjærestad, R. R. P. Singh, R. H. McKenzie, and R. Coldea, Phys. Rev. B **74**, 224420 (2006).
[44] Y. Zou and X.-G. Wen, arXiv:cond-mat/0210662.
[45] T. Herfurth, S. Streib, and P. Kopietz, Phys. Rev. B **88**, 174404 (2013).